

# Ultrasensitive Proximity Josephson Sensor with Kinetic Inductance Read-Out

F. Giazotto,<sup>1,\*</sup> T. T. Heikkilä,<sup>2</sup> G. Pepe,<sup>3</sup> P. Helistö,<sup>4</sup> A. Luukanen,<sup>5</sup> and J. P. Pekola<sup>2</sup>

<sup>1</sup>*NEST CNR-INFM and Scuola Normale Superiore, I-56126 Pisa, Italy*

<sup>2</sup>*Low Temperature Laboratory, Helsinki University of Technology, P.O. Box 3500, FIN-02015 TKK, Finland*

<sup>3</sup>*CNR-INFM Coherentia and Dipartimento Scienze Fisiche, Università di Napoli "Federico II," Monte Sant'Angelo, I-80125 Napoli, Italy*

<sup>4</sup>*VTT Information Technology, Tietotie 3, Fin-02150 Espoo, Finland*

<sup>5</sup>*Millilab, VTT, Tietotie 3, Fin-02150 Espoo, Finland*

We propose a mesoscopic kinetic-inductance radiation detector based on a long superconductor-normal metal-superconductor Josephson junction. The operation of this proximity Josephson sensor (PJS) relies on large kinetic inductance variations under irradiation due to the exponential temperature dependence of the critical current. Coupled with a dc SQUID readout, the PJS is able to provide a signal to noise (S/N) ratio up to  $\sim 10^3$  in the THz regime if operated as calorimeter, while electrical noise equivalent power (NEP) as low as  $\sim 7 \times 10^{-20}$  W/ $\sqrt{\text{Hz}}$  at 200 mK can be achieved in the bolometer operation. The high performance together with the ease of fabrication make this structure attractive as an ultrasensitive cryogenic detector of THz electromagnetic radiation.

PACS numbers: 85.25.Oj, 74.45.+c, 73.23.-b, 73.50.Lw

Superconducting single-photon detectors [1, 2, 3] offer high infrared detection efficiency, high-speed timing resolution and few-nanosecond reset times. They have been applied in several fields including spectroscopy of ultrafast quantum phenomena [4], optical communications [5], quantum cryptography [6], and fast digital circuit testing [7]. On the other hand, a wide potential for superconducting nanoscale detectors used as advanced bolometers is also expected in several astrophysical space applications, where bolometers are promising candidates to meet future needs of cooled telescopes. The interest lies in the negligible Johnson noise they show with a NEP as low as  $10^{-18}$  W/ $\sqrt{\text{Hz}}$ . Hot-electron resistive microbolometers and kinetic inductance superconducting detectors (KIDs) represent high performance devices able to reach  $\text{NEP} \lesssim 10^{-19}$  W/ $\sqrt{\text{Hz}}$  at  $T \geq 1$  K [8]. KIDs [9] offer about the same NEP and response time as resistive bolometers and hot electron detectors, and they can operate at temperatures much below the critical temperature where the generation-recombination noise is small thanks to the reduced number of quasiparticles.

Here we propose a KID based on a long superconductor-normal metal-superconductor Josephson junction. It exploits large kinetic inductance variations under irradiation thanks to the exponential temperature dependence of the supercurrent, and yields a high S/N ratio ( $\sim 10^3$  around 40 THz) and a low NEP ( $\sim 7 \times 10^{-20}$  W/ $\sqrt{\text{Hz}}$  at 200 mK). The ease of implementation combined with large array scalability make this structure promising as a sub-Kelvin ultrasensitive detector of far- and mid-infrared electromagnetic radiation.

The structure we envision is sketched in Fig. 1(a) and consists of a diffusive normal metal (N) wire of length  $l$  coupled to two superconducting leads (S) through transparent contacts, thus realizing a SNS Josephson weak link. An antenna eventually couples the incident radi-

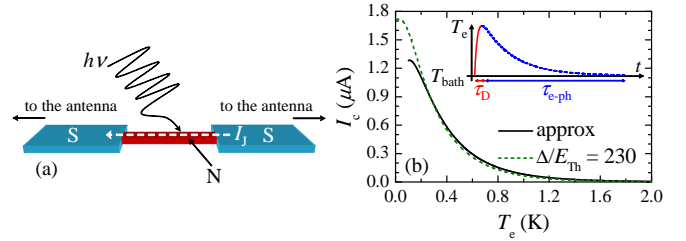


FIG. 1: (color online) (a) Scheme of the PJS. Incident electromagnetic radiation elevates the electron temperature ( $T_e$ ) in the N wire, thus strongly suppressing the Josephson current. This leads to a large enhancement of the junction kinetic inductance. (b) Supercurrent  $I_c$  vs electron temperature  $T_e$  of a long SNS Josephson junction calculated at  $\phi = \pi/2$  from Eq. (1) (full line), and for  $\Delta/E_{\text{Th}} = 230$  (dashed line). The inset shows a sketch of time evolution of  $T_e$  after absorption of radiation (see text).

ation to the N wire. We assume that the Josephson junction is long, i.e.,  $\Delta \gg \hbar D/l^2 = E_{\text{Th}}$ , where  $\Delta$  is the S gap,  $D$  is the diffusion coefficient of N, and  $E_{\text{Th}}$  is the Thouless energy. The radiation coupled to the junction heats the electrons in N to temperature  $T_e$ . For  $E_{\text{Th}} \ll k_B T_e \ll \Delta$ , the Josephson current is  $I_J = I_c \sin(\phi)$ , where  $\phi$  is the phase difference across superconductors, and [10]

$$I_c = \frac{64\pi k_B T_e}{(3 + 2\sqrt{2})eR_N} \sqrt{\frac{2\pi k_B T_e}{E_{\text{Th}}}} \exp\left(-\sqrt{\frac{2\pi k_B T_e}{E_{\text{Th}}}}\right) \quad (1)$$

is the junction critical current. Hence, in this limit,  $I_c$  depends exponentially on the electron temperature and is independent of the phonon temperature  $T_{\text{bath}}$ . In Eq. (1),  $R_N = \rho l/A$  is the normal-state resistance of the junction,  $\rho = (\nu_F e^2 D)^{-1}$  is the wire resistivity,  $A$  its cross section, and  $\nu_F$  is the density of states at the Fermi level in N. For our simulation we choose a 10-nm-thick silver (Ag) wire

with  $l = 1\mu\text{m}$ , width of 100 nm (volume  $\Omega = 10^{-21}\text{ m}^3$ ),  $\nu_{\text{F}} = 1.0 \times 10^{47}\text{ J}^{-1}\text{m}^{-3}$ , and  $D = 0.01\text{ m}^2\text{s}^{-1}$ . With the aforementioned parameters  $R_{\text{N}} \simeq 38\Omega$ , and  $E_{\text{Th}} \simeq 6.6\mu\text{eV}$ . By choosing, for instance, Nb as S electrodes ( $\Delta = 1.52\text{ meV}$ ) we get  $\Delta/E_{\text{Th}} \simeq 230$ , thus providing the frame of the *long* junction limit. The critical current  $I_{\text{c}}$  vs  $T_{\text{e}}$  is shown in Fig. 1(b) for  $\phi = \pi/2$  and  $\Delta/E_{\text{Th}} = 230$  (dashed line). In our case,  $I_{\text{c}}$  saturates around  $1.7\mu\text{A}$  at  $T_{\text{e}} \simeq 50\text{ mK}$ , and is suppressed by a factor of  $\sim 20$  at 1 K due to the exponential dependence on  $T_{\text{e}}$ . For a comparison, the approximated result from Eq. (1) is also shown (full line), and will be used in the following. Such suppression of  $I_{\text{c}}$  produces a large enhancement of the junction kinetic inductance ( $L_{\text{k}}$ ), defined as  $L_{\text{k}} = \hbar/(2eI_{\text{c}})$ . As we shall show, measuring  $L_{\text{k}}$  variations with a suitable readout scheme allows to accurately detect the radiation absorbed by the SNS junction.

In order to understand the operation principle of the PJS as a calorimeter (i.e., in pulsed excitation operation) as well as a bolometer (i.e., in continuous excitation operation) it is useful to consider the inset of Fig. 1(b), which shows a sketch of time evolution of  $T_{\text{e}}$  in N after the arrival of a photon. We assume that  $T_{\text{e}}$  is elevated with respect to  $T_{\text{bath}}$ , depending on the energy of the impinging photon and uniformly along N, over a time scale set by the diffusion time  $\tau_{\text{D}} = l^2/D$  [see the red line in the inset of Fig. 1(b)]. With our parameters  $\tau_{\text{D}} = 10^{-10}\text{ s}$ . Then, after the absorption of a photon,  $T_{\text{e}}$  relaxes toward  $T_{\text{bath}}$  over a time scale set by the electron-phonon interaction time ( $\tau_{\text{e-ph}}$ ), given by  $\tau_{\text{e-ph}} = 1/(\alpha T_{\text{bath}}^3)$  [11], where  $\alpha \approx 0.34\Sigma/(k_{\text{B}}^2\nu_{\text{F}})$ , and  $\Sigma$  is the electron-phonon coupling constant. By setting  $\Sigma = 5 \times 10^8\text{ Wm}^{-3}\text{K}^{-5}$ , as appropriate for Ag [11],  $\tau_{\text{e-ph}} \sim 1 \times 10^{-4} \dots 1 \times 10^{-7}\text{ s}$  in the  $0.1 \dots 1.0\text{ K}$  temperature range, so that  $\tau_{\text{e-ph}} \gg \tau_{\text{D}}$  [see the blue line in the inset of Fig. 1(b)]. In the following we analyze both the pulsed and the continuous excitation mode of the PJS.

In the pulsed mode, after the arrival of a photon of frequency  $\nu$  at time  $t = 0$ , the electron temperature in N can be determined by solving the heat equation  $C_{\text{e}}(\partial T_{\text{e}}/\partial t) = P_{\text{opt}}$  [11], where  $C_{\text{e}} = (\pi^2\nu_{\text{F}}k_{\text{B}}^2T_{\text{e}})/3$  is the electron heat capacity, and  $P_{\text{opt}} = (2\pi\hbar\nu/\Omega)\delta(t)$  is the optical input power per volume per incident photon. In writing the heat equation we neglected the spatial dependence of  $T_{\text{e}}$  in N, as well as the interaction with the lattice phonons, the latter occurring on a time scale  $\tau_{\text{e-ph}} \gg \tau_{\text{D}}$ . From the solution of the heat equation we get  $T_{\text{e}}(\nu) = \sqrt{T_{\text{bath}}^2 + 12\hbar\nu/(\pi\Omega\nu_{\text{F}}k_{\text{B}}^2)}$ , which shows that small N volumes are required to achieve large enhancement of  $T_{\text{e}}$ . This condition can be easily met in metallic SNS junctions, where N island with volumes below  $10^{-21}\text{ m}^3$  can be routinely fabricated with the present technology. The relative variation of the kinetic inductance, i.e., the quantity  $\delta L_{\text{k}}/L_{\text{k}}^0 = [L_{\text{k}}(\nu) - L_{\text{k}}(0)]/L_{\text{k}}(0)$  is displayed in Fig. 2(a) as a function of  $\nu$  at different  $T_{\text{bath}}$ . In the present structure,  $\delta L_{\text{k}}/L_{\text{k}}^0$  of about 14%

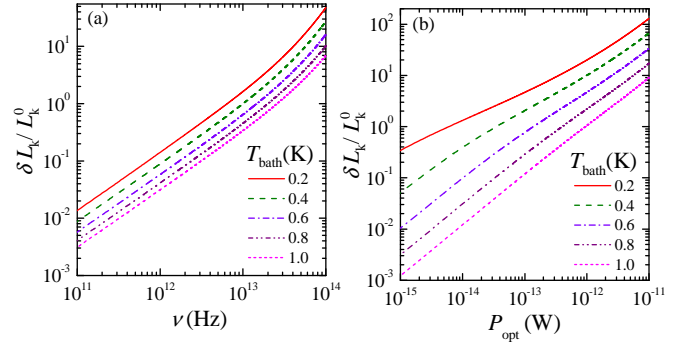


FIG. 2: (color online) (a)  $\delta L_{\text{k}}/L_{\text{k}}^0$  vs  $\nu$  at different  $T_{\text{bath}}$ . (b)  $\delta L_{\text{k}}/L_{\text{k}}^0$  vs  $P_{\text{opt}}$  calculated at different  $T_{\text{bath}}$ .

for 1 THz photon, and around 163% for 10 THz photon can be achieved at 200 mK. At higher bath temperatures  $\delta L_{\text{k}}/L_{\text{k}}^0$  is reduced, and obtains values of about 3% at 1 THz and around 35% at 10 THz at  $T_{\text{bath}} = 1\text{ K}$ . Such kinetic inductance variations allow for a very large signal to noise ratio for single-photon detection.

The PJS operation in continuous excitation can be described by considering those mechanisms which drive power into the N electrons. At low temperature (typically below 1 K), the main contribution in metals is related to electron-phonon heat flux which can be modeled by  $\dot{Q}_{\text{e-ph}} = \Sigma\Omega(T_{\text{e}}^5 - T_{\text{bath}}^5)$  [11]. The steady-state  $T_{\text{e}}$  under irradiation with a continuous power  $P_{\text{opt}}$  thus follows directly from the solution of the energy balance equation  $P_{\text{opt}} + \dot{Q}_{\text{e-ph}} = 0$ , which gives  $T_{\text{e}}(P_{\text{opt}}) = \sqrt[5]{(P_{\text{opt}}/\Sigma\Omega) + T_{\text{bath}}^5}$ . This expression shows that both reduced  $\Omega$  and small  $\Sigma$  are required to maximize  $T_{\text{e}}$  enhancement upon power irradiation. The impact of continuous power excitation on the junction kinetic inductance is shown in Fig. 2(b) which shows  $\delta L_{\text{k}}/L_{\text{k}}^0 = [L_{\text{k}}(P_{\text{opt}}) - L_{\text{k}}(0)]/L_{\text{k}}(0)$  versus  $P_{\text{opt}}$  at several  $T_{\text{bath}}$ . Notably,  $\delta L_{\text{k}}/L_{\text{k}}^0$  as large as  $\simeq 130\%$  for  $P_{\text{opt}} = 10\text{ fW}$  and  $\simeq 2000\%$  for  $P_{\text{opt}} = 1\text{ pW}$  at  $T_{\text{bath}} = 0.2\text{ K}$  can be achieved. At higher bath temperatures  $\delta L_{\text{k}}/L_{\text{k}}^0$  gets reduced, reaching values  $\simeq 1\%$  for  $P_{\text{opt}} = 10\text{ fW}$  and  $\simeq 100\%$  for  $P_{\text{opt}} = 1\text{ pW}$  at 1 K.

We now turn on discussing the PJS performance by considering a superconducting quantum interference device (SQUID) readout, as shown in Fig. 3(a) [12]. A constant bias current  $I_{\text{b}}$  divides into two parts, i.e., one flowing through the SNS junction [13], and the other ( $I_{\text{L}}$ ) through a load inductor ( $L$ ) coupled to a dc SQUID. Upon irradiation, an enhancement of  $L_{\text{k}}$  results in a variation of  $I_{\text{L}}$ , thus producing a magnetic field which is detected by the SQUID. The magnetic flux generated by the incident radiation is given by  $\Phi = MI_{\text{L}}$ , where  $M$  is the mutual inductance between the SQUID and the SNS junction loop. In the linearized regime, i.e., by assuming  $LI_{\text{L}} \ll \Phi_0$  where  $\Phi_0$  is the flux quantum, we get  $I_{\text{L}} \approx I_{\text{b}}\Phi_0/(\Phi_0 + LI_{\text{c}})$ , and  $dI_{\text{L}}/dI_{\text{c}} \approx LI_{\text{b}}\Phi_0/(\Phi_0 + LI_{\text{c}})^2$ .

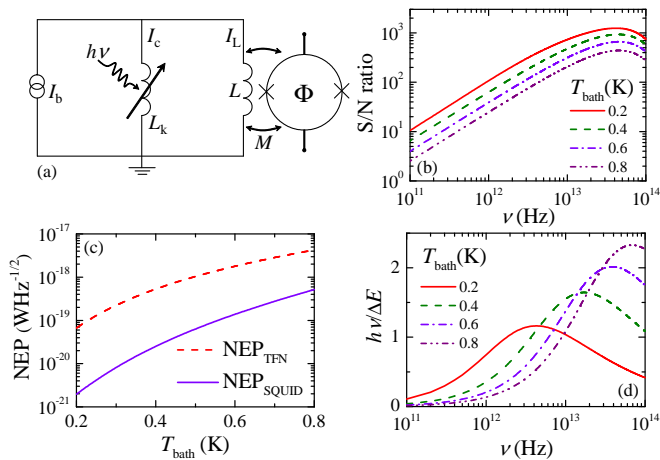


FIG. 3: (color online) (a) Scheme of the KID with a dc SQUID readout. (b) S/N ratio vs  $\nu$  calculated at different  $T_{\text{bath}}$ . (c) Temperature dependencies of NEP due to thermal fluctuation noise (TFN) and to the SQUID readout. (d) Resolving power vs  $\nu$  calculated at different  $T_{\text{bath}}$ .

In the pulsed detection mode, the signal to noise ratio (S/N) can be readily expressed as

$$\frac{S}{N} = \frac{(d\Phi/dT_e)\delta T_e}{\delta\Phi_n\sqrt{\omega}} = \left| \frac{M(dI_L/dI_c)(dI_c/dT_e)\delta T_e}{\delta\Phi_n\sqrt{\omega}} \right|, \quad (2)$$

where  $\delta\Phi_n$  is the flux sensitivity of the dc SQUID, and  $\omega$  its bandwidth. The S/N ratio versus  $\nu$  is shown in Fig. 3(b) at different  $T_{\text{bath}}$ . Here we set  $L = 100$  nH,  $M = 10$  nH,  $\omega = 1$  MHz,  $\delta\Phi_n = 10^{-7}\Phi_0/\sqrt{\text{Hz}}$  [14], and  $I_b = 0.8I_c(\nu)$ . Notably, very high S/N ratios can be achieved with the PJS in the 100 GHz - 100 THz frequency range. The S/N ratio is maximized around 40 THz where it obtains values  $\sim 1.2 \times 10^3$  at  $T_{\text{bath}} = 0.2$  K. In the bolometer operation, on the other hand, an important figure of merit is the NEP, which is due to several uncorrelated noise sources. In our case, the dominant contribution is due to thermal fluctuation noise-limited NEP (NEP<sub>TFN</sub>), given by  $\text{NEP}_{\text{TFN}} = \sqrt{5k_B\Sigma\Omega(T_e^6 + T_{\text{bath}}^6)}$  [11], while the contribution due to Johnson noise is absent, thanks to the operation of the junction in the dissipationless regime. The contribution of the SQUID readout to NEP (NEP<sub>SQUID</sub>) can be determined by setting  $S/N = 1$ ,  $\omega = 1$  Hz, and solving Eq. (2) for  $P_{\text{opt}}$ . Figure 3(c) shows the NEP<sub>TFN</sub> (dashed line) and NEP<sub>SQUID</sub> (full line) vs  $T_{\text{bath}}$ . NEP<sub>SQUID</sub> is significantly smaller than NEP<sub>TFN</sub>, and the latter can be as low as  $\simeq 7 \times 10^{-20}$  W/ $\sqrt{\text{Hz}}$  at 0.2 K. Further reduction of NEP<sub>TFN</sub> is possible by lowering  $\Omega$  as well as by exploiting materials with lower  $\Sigma$ . Above, we have discussed the electrical NEP — the optical NEP is of the same order of magnitude. This is because the resistance of the device can be easily matched to common broadband self-similar lithographic antennas. The PJS resolving power ( $2\pi\hbar\nu/\Delta E$ ) vs frequency, where  $\Delta E \approx 2\sqrt{2\ln 2\text{NEP}_{\text{TFN}}(\nu)}\sqrt{\tau_{\text{e-ph}}}$  is the en-

ergy resolution of full width at half maximum [11], is displayed in Fig. 3(d) for different  $T_{\text{bath}}$ . In particular, the figure shows that resolving power values between  $\sim 1.2$  and  $\sim 2.3$  can be achieved in the 5...70 THz frequency range for  $T_{\text{bath}} \gtrsim 400$  mK, thus making the PJS suitable for *far-* and *mid-infrared* single-photon detection.

The mechanism for the supercurrent in SNS junctions is due to the proximity effect, giving rise in the N local density of states to an energy minigap of size  $E_g = c(\phi)E_{\text{Th}}$  with  $c(0) \approx 3.1$  [15], which we have ignored in the expressions for the heat capacity and electron-phonon coupling. Due to the minigap, both of these quantities are reduced inside the N wire, further improving the device resolution. Moreover, the density of states is not divergent at the minigap edge, contrary to bulk superconductors, and thereby the generation-recombination noise is reduced. For the chosen parameters the minigap  $E_g \sim \hbar \cdot 5$  GHz, and thereby radiation from low frequencies  $\nu < E_g/\hbar$ , which typically is not part of the measured signal, should not couple in the device.

In summary, we have analyzed a proximity Josephson sensor (PJS) based on a long SNS junction in the kinetic inductance mode. Signal-to-noise ratio as high as  $\sim 10^3$  and noise equivalent power below  $10^{-19}$  W/ $\sqrt{\text{Hz}}$  at 0.2 K have been found to be achievable. Together with the available resolving power, the PJS is a promising candidate for single-photon detection in the THz regime.

We thank the NanoSciERA "NanoFridge" project and the Academy of Finland for financial support.

\* Electronic address: [giazotto@sns.it](mailto:giazotto@sns.it)

- [1] A. J. Kerman, E. A. Dauler, W. E. Keicher, J. K. W. Yang, K. K. Berggren, G. N. Gol'tsman, and B. M. Voronov, *Appl. Phys. Lett.* **88**, 111116 (2006).
- [2] G. Gol'tsman, O. Okunev, G. Chulkova, A. Lipatov, A. Dzardanov, K. Smirnov, A. Semenov, B. Voronov, C. Williams, and R. Sobolewski, *IEEE Trans. Appl. Supercond.* **11**, 574 (2001).
- [3] A. A. Houck, D. I. Schuster, J. M. Gambetta, J. A. Schreier, B. R. Johnson, J. M. Chow, L. Frunzio, J. Majer, M. H. Devoret, S. M. Girvin, and R. J. Schoelkopf, *Nature* **449**, 328 (2007).
- [4] M. A. Jaspán, J. L. Habif, R. H. Hadfield, and S. W. Nam, *Appl. Phys. Lett.* **89**, 031112 (2006).
- [5] S. Robinson, A. J. Kerman, E. A. Dauler, R. J. Barron, D. O. Caplan, M. L. Stevens, J. J. Carney, S. A. Hamilton, J. K. W. Yang, and K. K. Berggren, *Opt. Lett.* **31**, 444 (2006).
- [6] S. Benjamin, *Science* **290**, 2273 (2000).
- [7] A. Korneev, A. Lipatov, O. Okunev, G. Chulkova, K. Smirnov, G. Gol'tsman, J. Zhang, W. Slysz, A. Verevkin, and R. Sobolewski, *Microelectron. Eng.* **69**, 274 (2003).
- [8] A. V. Sergeev, V. V. Mitin, and B. S. Karasik, *Appl. Phys. Lett.* **80**, 817 (2002); J. J. Bock, J. Glenn, S. M. Grannan, K. D. Irwin, A. E. Lange, H. G. LeDuc, and A. D. Turner, *Proc. SPIE* 3357, **297** (1998).

- [9] N. Grossman, D. G. McDonald, and J. E. Sauvageau, IEEE Trans. Magn. **27**, 2677 (1991); N. Bluzer and M. G. Forrester, Opt. Eng. **33**, 697 (1994).
- [10] A. D. Zaikin and G. F. Zharkov, Sov. J. Low Temp. Phys. **7**, 184 (1981); F. K. Wilhelm, A. D. Zaikin, and G. Schön, J. Low Temp. Phys. **106**, 305 (1997).
- [11] See F. Giazotto, T. T. Heikkilä, A. Luukanen, A. M. Savin, and J. P. Pekola, Rev. Mod. Phys. **78**, 217 (2006), and references therein.
- [12] The SQUID readout of the sensor can be implemented in a resonant circuit, and thereby multiplexed using standard SQUID multiplexing schemes, see for example T. M. Lanting, *et al.*, Appl. Phys. Lett. **86**, 112511 (2005).
- [13] The expressions concerning the read-out have been derived using the Josephson inductance model corresponding to the linearized current-phase relation. This allows for analytic expressions, but slightly underestimates the detector response.
- [14] M. Kiviranta, J. S. Penttilä, L. Grönberg, J. Hassel, A. Virtanen, and H. Seppä, Supercond. Sci. Technol. **17**, S285 (2004).
- [15] F. Zhou, P. Charlat, B. Spivak, and B. Pannetier, J. Low Temp. Phys. **110**, 841 (1998).